A Noninvasive Platform for Imaging and Quantifying Oil Storage in Submillimeter Tobacco Seed[1][W][OA]

Johannes Fuchs, Thomas Neuberger, Hardy Rolletschek, Silke Schiebold, Thuy Ha Nguyen, Nikolai Borisjuk, Andreas Börner, Gerd Melkus, Peter Jakob, and Ljudmilla Borisjuk*

Leibniz-Institut für Pflanzengenetik und Kulturpflanzenforschung, 06466 Gatersleben, Germany (J.F., H.R., S.S., A.B., L.B.); University of Würzburg, Institute of Experimental Physics 5, 97074 Wuerzburg, Germany (J.F., P.J.); The Huck Institutes of the Life Sciences and Department of Bioengineering, Pennsylvania State University, University Park, Pennsylvania 16802 (T.N.); Microbiologist (Atlanta Research and Education Foundation) Molecular Epidemiology Team, Influenza Division/National Center for Immunization and Respiratory Diseases, Centers for Disease Control and Prevention, Atlanta, Georgia 30333 (T.H.N.); Rutgers University, New Brunswick, New Jersey 08901 (N.B.); Department of Radiology and Biomedical Imaging, University of California, San Francisco, California 94107 (G.M.); and Research Center Magnetic Resonance Bavaria, 97074 Wuerzburg, Germany (P.J.)

While often thought of as a smoking drug, tobacco (*Nicotiana* spp.) is now considered as a plant of choice for molecular farming and biofuel production. Here, we describe a noninvasive means of deriving both the distribution of lipid and the microtopology of the submillimeter tobacco seed, founded on nuclear magnetic resonance (NMR) technology. Our platform enables counting of seeds inside the intact tobacco capsule to measure seed sizes, to model the seed interior in three dimensions, to quantify the lipid content, and to visualize lipid gradients. Hundreds of seeds can be simultaneously imaged at an isotropic resolution of 25 μm, sufficient to assess each individual seed. The relative contributions of the embryo and the endosperm to both seed size and total lipid content could be assessed. The extension of the platform to a range of wild and cultivated *Nicotiana* species demonstrated certain evolutionary trends in both seed topology and pattern of lipid storage. The NMR analysis of transgenic tobacco plants with seed-specific ectopic expression of the plastidial phospho*enol*pyruvate/phosphate translocator, displayed a trade off between seed size and oil concentration. The NMR-based assay of seed lipid content and topology has a number of potential applications, in particular providing a means to test and optimize transgenic strategies aimed at the manipulation of seed size, seed number, and lipid content in tobacco and other species with submillimeter seeds.

The use of tobacco (*Nicotiana* spp.) dates back to the Mayan civilization (Zagorevski and Loughmiller-Newman, 2012) and in modern times still retains a primary place, as measured by monetary value, among nonfood crop species. Given the well-documented health risks associated with smoking tobacco, finding alternative uses for the crop represents an active area of research. The ease of its genetic transformation (the species was the first plant to be successfully transformed some 30 years ago by Zambryski et al. [1983]) has prompted a suggestion that it might be used as a vehicle for the synthesis of high-value pharmaceutical compounds (Borisjuk et al., 1999; Davoodi-Semiromi et al., 2009; Morandini et al., 2011) and enzymes (Verma et al., 2010; Agrawal et al., 2011). Its potential biomass production can reach 170 tons ha^{-1} per year in some commercial varieties (Schillberg et al., 2003), a level that is attractive in the context of biofuel production (Usta, 2005; Andrianov et al., 2010).

Tobacco seed is conventionally considered to have no commercial use, but a production level of up to approximately 1.2 tons ha^{-1} has been documented in the literature (Patel et al., 1998). The seed contains as much as 40% lipid (Frega et al., 1991), consisting mainly of triacylglycerols with a predominant contribution, about 75%, of linoleic acid. Tobacco seed lipid can be blended with mineral diesel fuel without any need for engine modification or fuel preheating (Usta, 2005). The conversion of tobacco into an energy crop can take advantage of a well-developed biotechnology infrastructure (Gadani et al., 2003). Molecular markers have been applied to characterize the genetic diversity present in breeding germplasm (Ren and Timko, 2001; Fricano et al., 2012). Furthermore, a dense marker-based genetic map has been derived (Bindler et al., 2011), and substantial volumes of DNA sequences have been deposited in the public domain (www.pngg.org/tgi/).

Studying the biology of lipid deposition in tobacco seed (tissue specificity, seed size, and architecture) is hampered by the small size of the seed (typically <1 mm in diameter; Fig. 1A) and the large number of

[1] This work was supported by the German Plant Phenotyping Network.

* Corresponding author; e-mail borysyuk@ipk-gatersleben.de.

The author responsible for distribution of materials integral to the findings presented in this article in accordance with the policy described in the Instructions for Authors (www.plantphysiol.org) is: Ljudmilla Borisjuk (borysyuk@ipk-gatersleben.de).

[W] The online version of this article contains Web-only data.

[OA] Open Access articles can be viewed online without a subscription.

www.plantphysiol.org/cgi/doi/10.1104/pp.112.210062

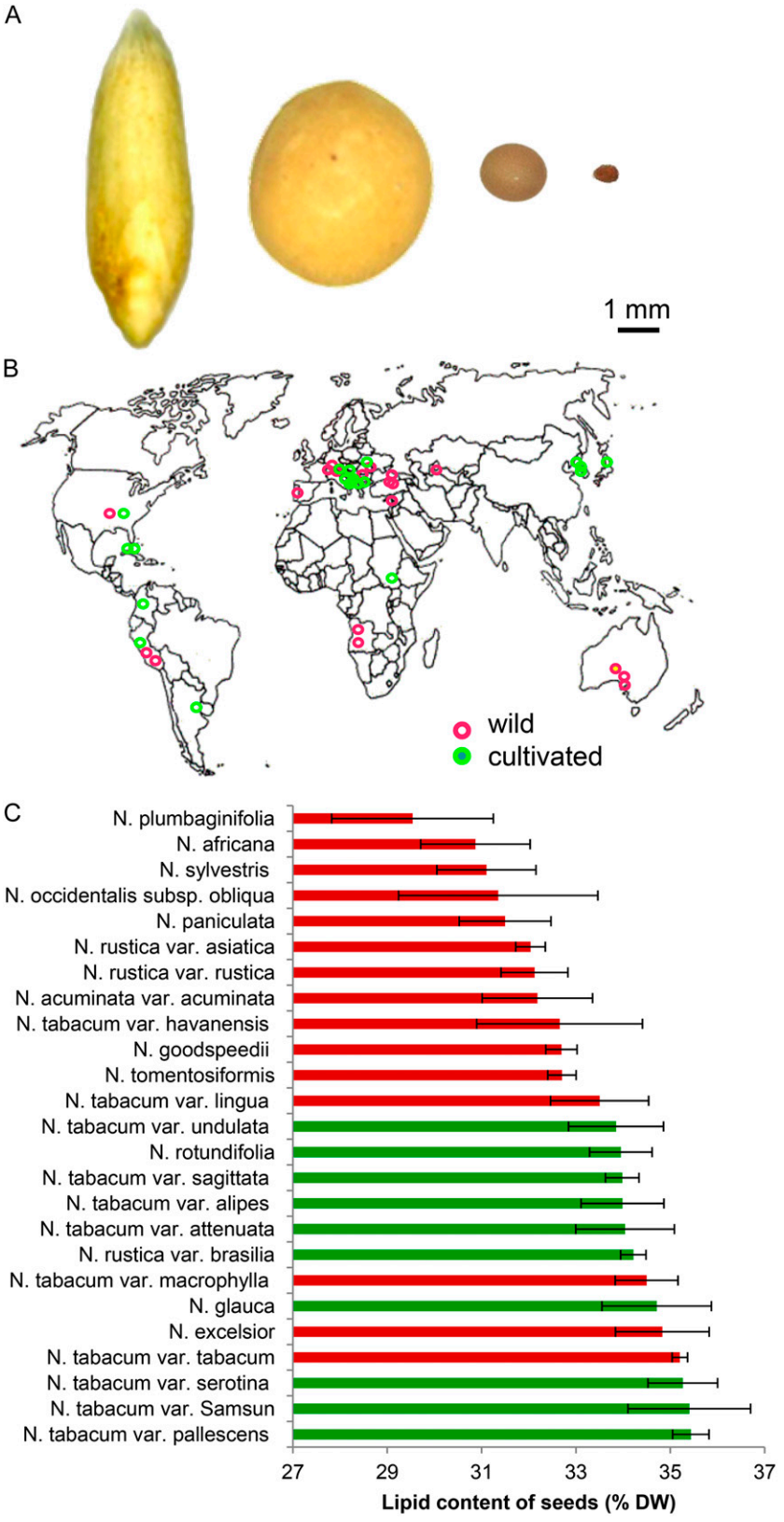

Figure 1. Variability in seed lipid content as estimated using TD-NMR in a range of *Nicotiana* species. A, Typical seed size of (from left to right) oat, soybean, oilseed rape, and tobacco. B, The geographical provenance of wild (red) and cultivated (green) *Nicotiana* spp. accessions. C, Seed lipid content expressed as a percentage of seed dry weight (DW).

seeds formed within each capsule. Preexisting approaches to characterize the internal structure of seeds and to quantify the lipid fraction within them (Borisjuk et al., 2011, 2012; Horn et al., 2011a, 2012) are not readily applicable to small seeds. To the best of our knowledge, there is no method available for the noninvasive lipid imaging in submillimeter oilseeds as those of the genus *Nicotiana*.

Our work describes how NMR can be exploited to provide a noninvasive platform for the in vivo analysis of tobacco seed. The method allows for both the characterization of seed architecture and the assessment of tissue-specific lipid storage capacity without any seed destruction. The simultaneous imaging of some hundreds of seeds can be achieved at a level of resolution sufficient to assess each seed individually. The method has been applied to investigate lipid deposition in the endosperm and embryo of the seed of various *Nicotiana* species as well as transgenic tobacco plants, thereby uncovering a previously unrecognized trade off between seed growth and lipid storage.

RESULTS

NMR Analysis Suggests That the Seed of Cultivated Tobacco Is More Lipid Rich Than That of Its Wild Relatives

To assess the diversity of lipid content within the seed of *Nicotiana* species, a set of 64 accessions held at the German Federal ex situ GenBank at Leibniz-Institut für Pflanzengenetik und Kulturpflanzenforschung was surveyed. The germplasm sample comprised at least three accessions of each of the 11 species and in 10 cultivars of *Nicotiana tabacum*, which originate from Europe, Asia, Africa, Australia, and the Americas (Fig. 1B; Supplemental Table S1). Seed lipid content was determined by applying low-field time domain NMR (TD-NMR), a high-throughput platform that avoids the need for prior extraction procedures. All of the seed samples were heavily pigmented, but they varied in shape from nearly globular to angular, in their surface patterning and in their weight (by up to 3-fold). The range in lipid concentration varied by around 6% dry weight, with the lowest level found in the seed of *Nicotiana plumbaginifolia* and the highest in *N. tabacum*. Overall, the seed lipid content of the cultivated species was higher than that of the wild species (Fig. 1C).

Magnetic Resonance Imaging Allows Structural and Chemical Imaging of the Intact Capsule

The conventional means of characterizing the internal structure of the capsule (Fig. 2A) usually requires its prior dissection. By using magnetic resonance imaging (MRI), the destruction of the capsule can be avoided. Furthermore, due to the different frequencies of the proton signals, images from water only and lipid only can be acquired. Suppressing one of the signals prior to the multislice imaging sequence by means of a frequency selective suppression module (Tkác et al., 1999) delivers an image derived entirely from the nonsuppressed signal. Thus, if the water signal is suppressed, the remaining signal reflects the distribution of lipid within the capsule/seeds and vice versa. The two-dimensional multislice imaging of the capsule was applied as described in "Materials and Methods." The internal structure of the immature capsule was readily visualized from the water signal, since this tissue is highly hydrated (Fig. 2B). At the mid storage stage, the structure is dominated by the placenta, which encloses the developing seeds within two symmetrical chambers. Compared with the water content of the placental parenchyma and the leaves, the vascular bundle within the placenta and the capsule wall had a particularly high water content. Suppression of the water signal in turn resolved the lipid content of the structure at 68-μm

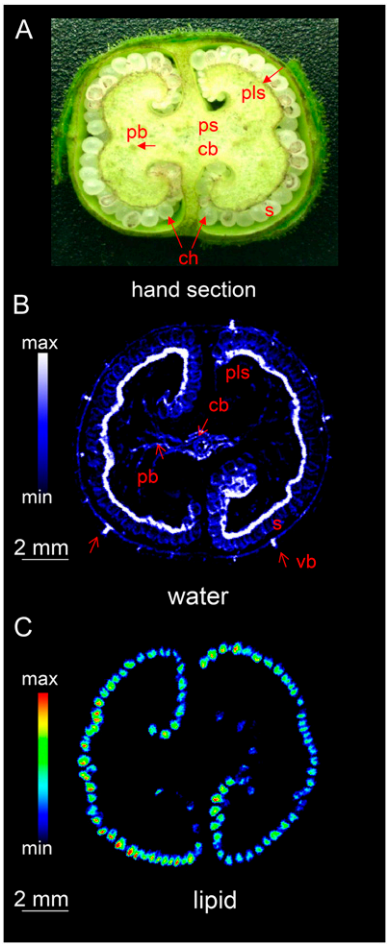

Figure 2. The internal structure of the tobacco capsule. A, Transverse section of the central portion, showing the arrangement of vascular bundles (hand-dissected capsule). B and C, MRI images showing the distribution of water (B) and lipids (C). cb, Central vascular bundle; pb, placental bundle; pls, placental surface; ps, placental stalk; S, seed; ch, chamber; vb, vascular bundle. See also Supplemental Movie S1.

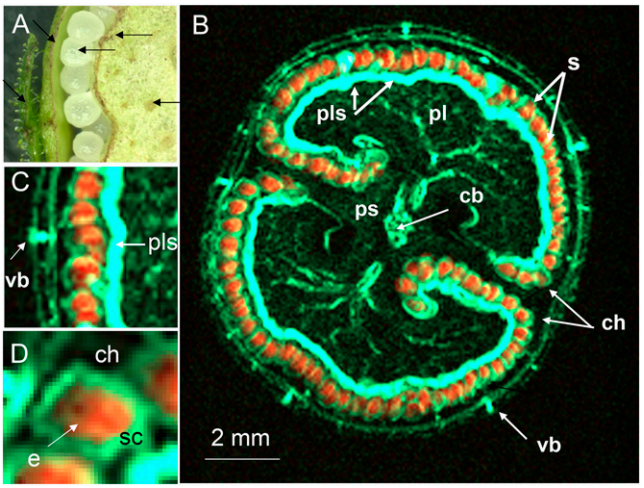

Figure 3. Integrated MRI overlaying the water and lipid distribution within an intact tobacco capsule. Hydrated tissue colored cyan and lipid-rich tissue orange. A, Fragment of cross section (hand-dissected capsule). B, Integrated MRI image. C, Enlargement of B showing lipid-rich seeds, vascular bundle, and placental surface. D, Enlargement of B showing lipid inside of seed and water-rich testa. e, Endosperm; sc, seed coat; other abbreviations as given in the legend to Figure 2.

isotropic resolution (Fig. 2C). The signal was mostly concentrated on the internal surface of the capsule, corresponding to the positions of the individual seeds (seen as rainbow-colored dots). An animated scan (Supplemental Movie S1) of an intact capsule illustrates its internal structure, in particular demonstrating the distribution of water (on the right) and the sites of lipid deposition (on the left). As the same capsule provided both sets of data, a virtual reconstruction of the capsule was straightforward to generate. The two-dimensional images shown in Figure 3 illustrate the architecture of the capsule during the main storage phase. The images integrating the water (colored cyan) and lipid (red) status (Fig. 3, B and C) indicate that the most heavily hydrated tissues were the placental vasculature and the regions in contact with the seeds, rather than the placenta itself. The thin water-rich layer inside the seed is the testa (Fig. 3D).

Three-Dimensional Modeling of the Capsule and the Estimation of the Seed Number

Our NMR platform also allows to image the intact capsule three dimensionally and to obtain a count of the seed. This was made possible by employing spin-echo imaging based solely on global chemical shift selective pulses. The details of this method are described in "Materials and Methods." A resulting three-dimensional reconstruction of the capsule is represented in Figure 4 (see also Supplemental Movie S2). The hydration level of the maternal tissues of the capsule was rather low, especially in the pericarp; the most hydrated portions of the capsule were the vascular bundles, the placental stalk, and the placental bundles. As individual seeds could be readily identified, the number of seeds within the imaged capsule was estimated without a destructive assay. Specifically, the seed count was achieved by dividing the combined volume of lipid filled pixels (derived from the lipid image) by the mean volume of each seed (determined from five manually segmented seeds). The resulting seed number per capsule was 413 ± 37.

Microimaging of Lipids within the Embryos and Endosperms of Intact Seeds

The testa of the mature tobacco seed normally renders the endosperm and embryo inaccessible except by destructive assay (Fig. 5A). High-resolution three-dimensional imaging and modeling of the mature tobacco seed was achieved by using high-field MRI (17.6 Tesla) in combination with a custom-built 2-mm-i.d. solenoid coil as a detector. This procedure compromised neither the subsequent germination performance nor the plant growth (data not shown). A standard three-dimensional spin-echo sequence was used to acquire a three-dimensional image of the lipid distribution (see "Materials and Methods") within the seed, followed by image segmentation in order to relate the distribution of the NMR signal to individual organs (Melkus et al., 2009). The model shown in Figure 5B, which features both the endosperm and the embryo, allowed their respective volumes to be estimated. This allows accurate calculation of the endosperm/embryo ratios as well as estimation of their contribution to seed biomass. The distribution of lipid could be assessed at 25-μm isotropic resolution as is illustrated in Figure 5, C to E (see also Supplemental Movies S3–S5). Lipid levels appeared to be highest in the endosperm, a

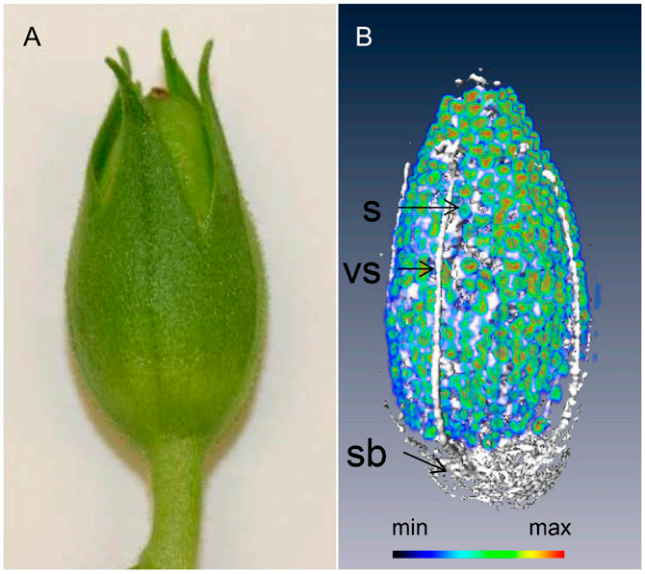

Figure 4. MRI visualization of the development of the tobacco capsule. A, Freshly harvested tobacco capsule. B, Three-dimensional reconstruction, showing the distribution of water (white) and lipid (rainbow) in an intact capsule (21 d after fertilization). The intensity of the lipid specific signal is color coded. vs, Vascular bundle; sb, stalk base; S, seed. See also Supplemental Movie S2.

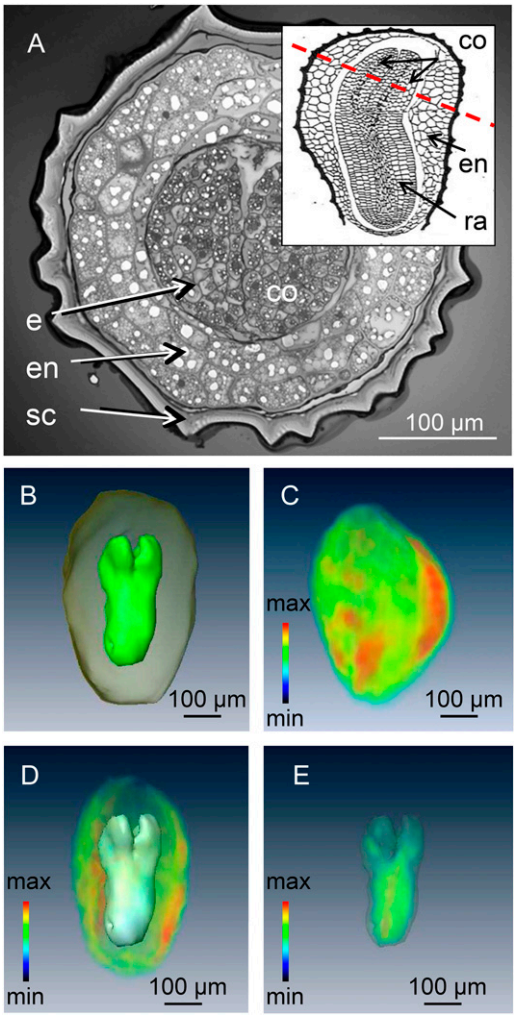

Figure 5. Conventional and MRI visualization of the interior of a tobacco seed. A, Cross section through the mature seed showing the cotyledons surrounded by the endosperm and the seed coat. The inset shows a longitudinal view, illustrating the plane of the cross section. B, NMR-based model of the embryo and endosperm. C, Three-dimensional visualization of lipid distribution within a single seed. D, The lipid profile of the endosperm. E, The lipid profile of the embryo; signal intensity (relative units) indicated by color coding with maximum in red. co, Cotyledon; e, embryo; en, endosperm; ra, radical; sc, seed coat. See also Supplemental Movies S3 to S5.

structure composed of larger cells than are present in the embryo (Fig. 5A). Lipid deposition in the embryo was associated with the radicle rather than with the cotyledon (Fig. 5E), and no lipid was deposited in the testa.

Cross-Species Comparison of Seed Architecture and Lipid Distribution

The NMR method in principle enabled a cross-species comparison to be made of seed architecture and lipid distribution. For this purpose, we performed a calibration of the lipid signal (see "Materials and Methods") and applied this improved measurement scheme to individual seeds of cultivated *N. tabacum* and wild species *Nicotiana sylvestris* and *Nicotiana tomentosiformis* (considered as ancestors; Ren and Timko, 2001). Comparisons between *N. sylvestris* or *N. tomentosiformis* and *N. tabacum* showed that the former formed smaller seeds and distinct morphology (Fig. 6, A–C). The indication from the NMR-based, three-dimensional reconstructions was that for all three species the volume of the embryo was less than that of the endosperm (Fig. 6, D–F). The ratio between these two volumes was 6.2 in *N. tabacum* but much higher in *N. sylvestris* (14.4) and *N. tomentosiformis* (22.7). However, the distribution of lipids in the embryo was similar among all three species, in each case showing a degree of preferential accumulation in the radicle (Fig. 6, G–I), although most of the lipid was deposited in the endosperm (Fig. 6,

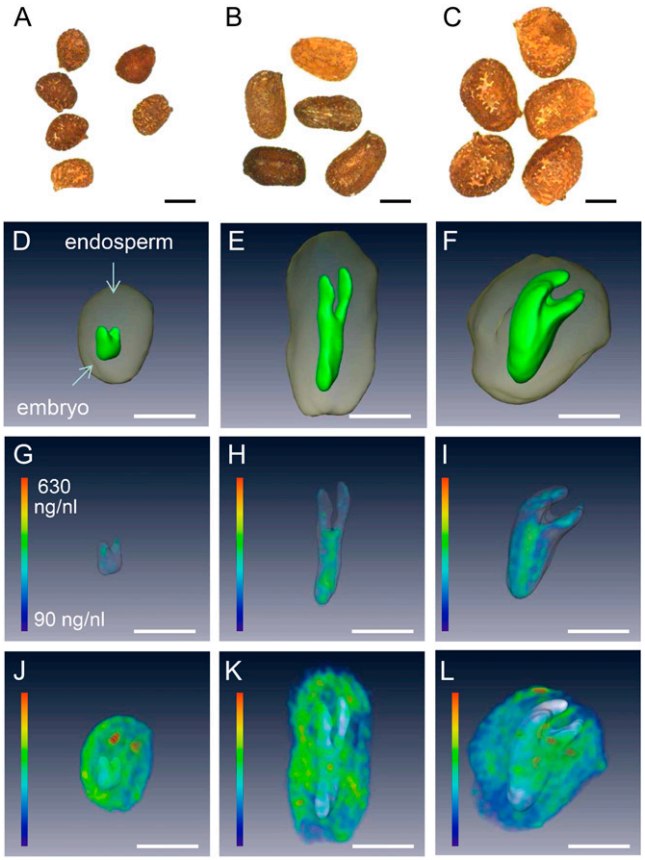

Figure 6. MRI visualization of the distribution of lipids within an individual seed of *N. tomentosiformis* (A, D, G, and J), *N. sylvestris* (B, E, H, and K), and *N. tabacum* (C, F, I, and L). A to C, An intact seed as used for imaging. D to F, Three-dimensional model showing the embryo (green) surrounded by the endosperm (gray). G to I, Three-dimensional visualization of lipid distribution within the embryo. J to L, Three-dimensional visualization of lipid distribution within the endosperm. Lipid concentration (μL ng^{-1}) indicated by color coding as shown in G. Bars = 200 μm.

J–L). The lipid concentration in both the embryo and endosperm was invariant across the three species.

Heterologous Expression of BoPPT1 in Tobacco Seed Alters the Pattern of Lipid Accumulation

The *Brassica oleracea* gene *BoPPT1* encodes the plastidial phospho*enol*pyruvate/phosphate translocator PPT1, a protein that plays a role in lipid storage (Schwender and Ohlrogge, 2002; Andre and Benning, 2007). In tobacco plants where *BoPPT1* was driven by the seed-specific promoter *LegB4*, the transgene was activated most strongly during the main storage phase (Supplemental Fig. S1A). The wild type and the transgenic lines were not differentiated with respect to their pattern of lipid accumulation during seed development (Supplemental Fig. S1B). However, by seed maturity, the lipid content of the latter was statistically greater (up to 13%) than that of the wild type, while at the same time, there was no significant alteration in fatty acid composition (Supplemental Fig. S1C).

Method Design for Simultaneous Monitoring of a Large Number of Seeds

Having demonstrated that the heterologous expression of BoPPT1 in the seed had a positive impact on lipid accumulation, it was of interest to elucidate which organ was responsible for this effect. This required the simultaneous high-resolution imaging of many seeds. NMR-based imaging is a priori taken as less reasonable for screening tasks due to its low sample throughput. To overcome this limitation here, we developed a novel approach by three-dimensional imaging of multiple seeds and computation of the virtual model seeds (see "Materials and Methods"). Again high-field-strength MRI was used. A small tube containing 99 seeds of a BoPPT1 transgenic line (PPT7) was inserted into a larger tube containing 138 wild-type seeds. The position and size of the wild-type (dark gray) and transgenic (light gray) seeds is illustrated in Figure 7A and the schematic tissue pattern of the seed in Figure 7B. To derive the probable pattern of lipid distribution within each genotype, one virtual model was generated from the signal derived from all the 99 transgenic seeds (Fig. 7C) and a second from all the 138 wild-type seeds (Fig. 7D). When the tissue scheme was merged with the virtual lipid models to highlight the effect of the transgene, it was apparent that the increased quantity of lipid accumulated by the transgenic seed was accompanied by an altered lipid concentration in both the embryo and the endosperm. In the former, most of the alteration was associated with the hypocotyl/radicle, while in the latter it was the region surrounding the embryo that was the most affected. In addition, it was observed that the transgenic seeds were approximately 19% smaller than the wild-type ones and that their lipid content was approximately 13% higher. The transgenic seeds varied with respect to size by a factor of about two, and their size was inversely proportional to their lipid concentration (Fig. 7E). An equivalent correlation was not obvious among the wild-type seeds (Fig. 7F).

DISCUSSION

In this work, we propose to use NMR as a noninvasive platform for the multicomponent analysis of submillimeter seeds in vivo. We demonstrate how to count seeds inside the intact tobacco capsule, measure seed sizes, model the seed interior, quantify lipid content, and visualize lipid distribution. Using our approach, hundreds of seeds can be imaged simultaneously.

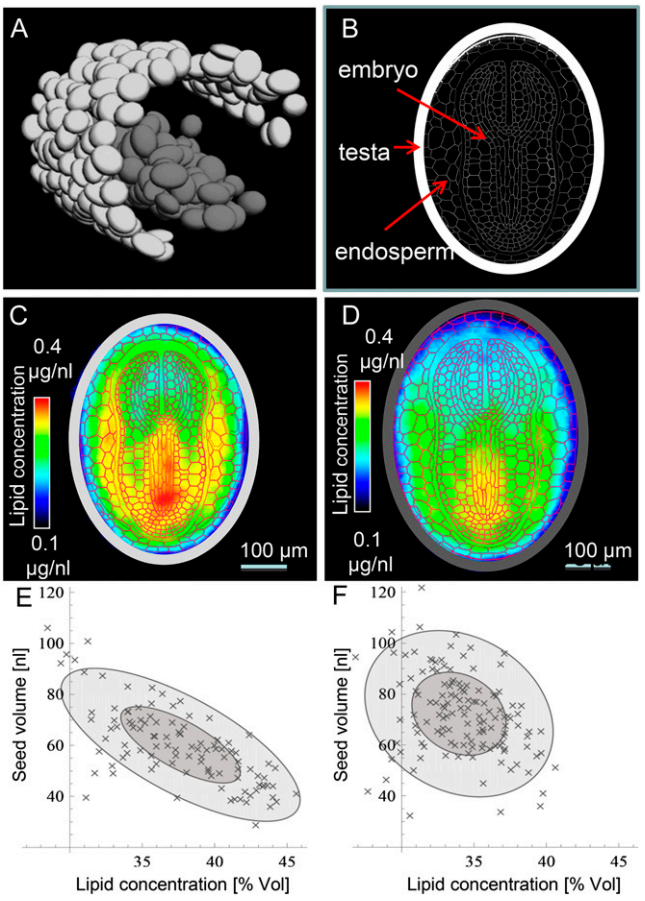

Figure 7. High-throughput MRI visualization and quantification of lipid content in intact tobacco seeds. A, The wild type (dark gray) and transgenic (light gray) "virtual seed" inside the NMR tubes. B, Arrangement of tissues within the tobacco seed. C and D, A representative transgenic (C) and wild-type (D) virtual model seed. E and F, Relationship between seed size and lipid content (given in percentage of volume) along an individual transgenic (E) and wild-type (F) seed. The size of the ellipses is determined by SD of the principal components (dark gray 1 σ; light gray 2 σ), and the obliqueness of the ellipse indicates the correlation between the size and the lipid concentration of the seed specimen.

These high-resolution NMR methods are a significant step toward the most wanted applications for the model plant Arabidopsis (*Arabidopsis thaliana*), where numerous oil storage mutants are available (Baud and Lepiniec, 2009; Wallis and Browse, 2010).

NMR Is a Versatile Tool for in Vivo Analysis of Tobacco Seeds

While the application to date of NMR to study seed biology has been productive (for review, see Borisjuk et al., 2012), the focus so far has been on large-seeded species, such as *Cocos nucifera*, *Arachis hypogaea*, *Pinus monticola*, and others (Table I). Because the sample size is of matter in NMR hardware design, submillimeter seeds remained challenging for being imaged using MRI. Thus, the seeds of tobacco and Arabidopsis (both of which are well established as model species) have so far remained inaccessible. To the best of our knowledge, only few NMR studies were devoted to small seeds (Manz et al., 2005; Seongjin, 2008), but despite their technical advance, they were not quit appropriate either for lipid detection or for detailed topological studies. In contrast, our protocols have been able to image individual tobacco seeds and their major internal organs. The combination of a high-throughput quantitative measurement of lipid facilitated by low-field TD-NMR and imaging based on high-field MRI has succeeded in a simultaneous imaging of hundreds of seeds in a way in which seed size and lipid content could be assessed on an individual seed basis. The level of resolution achieved (25 μm isotropic) was as much as 100-fold above that obtained by MRI as practiced in the clinical field (Table I). The data captured from hundreds of seeds could be integrated to produce a model of an individual seed reflecting an averaged lipid distribution (Fig. 7). The way is now open to applying MRI to small seeds to derive data with respect to seed composition and internal structure.

MRI Analysis Provides Insights into Lipid Topology in the Tobacco Seed

The topology of lipid accumulation in the seed is conventionally obtained using destructive sampling, and only few techniques are capable of tissue-specific analysis (Schiebold et al., 2011; Horn et al., 2012). The noninvasive NMR approach, extended here to small seeds, has demonstrated the internal distribution of lipid within the seed and has allowed for an evaluation of the relative contribution of the embryo and the endosperm to the overall quantity of lipid accumulated by the seed. We have shown that as in other crop species, tobacco accumulates lipid in both its endosperm and embryo, a pattern that concurs with the outcome of conventional studies (Tomlinson et al., 2004). At maturity, a nonuniform distribution of lipid in both the endosperm and the embryo (Fig. 5) was observed, providing evidence for a spatial incongruity in lipid storage activity during seed development. While the pattern of lipid deposition varied from seed

Table I. *NMR-based imaging of storage lipids among differently sized seeds*

Plant Species	Seed Size	Method	Field Strength (Proton Frequency)	Resolution (Slice Thickness)	Reference
	mm				
Coconut fruit (*Cocos nucifera*)	175	T1/T2-weighted spin echo imaging	9.4 Tesla (400 MHz)	781 × 781 μm^2 (3 mm)	Jagannathan et al. (1995)
Pecan seed (*Carya illinoinensis*)	40	Chemical shift imaging	4.7 Tesla (200 MHz)	800 × 800 μm^2 (No slice selection)	Halloin et al. (1993)
Groundnut (*Arachis hypogaea*)	9	Chemical shift selective spin-echo imaging	9.4 Tesla (400 MHz)	78 × 78 μm^2 (500 μm)	Lakshminarayana et al. (1992)
Wheat grain (*Triticum aestivum*)	7	Spin-echo imaging on dry seeds	20 Tesla (850 MHz)	35 μm isotropic	Borisjuk et al. (2011)
Pine seed (*Pinus monticola*)	6	Chemical shift-selective imaging	8.5 Tesla (360 MHz)	78 × 78 μm^2 (500 μm)	Terskikh et al. (2005)
Soybean seed	6	Spin-echo imaging on mature seeds	17.6 Tesla (750 MHz)	39 μm isotropic	Borisjuk et al. (2005)
Olives fruit (*Olea europaea*)	6	Chemical shift-selective spin-echo imaging	4.7 Tesla (200 MHz)	195 × 195 μm^2	Brescia et al. (2007)
Barley grain	5	Chemical shift-selective spin-echo imaging	17.6 Tesla (750 MHz)	31 × 31 μm^2 (750 μm)	Neuberger et al. (2008)
Cotton seed	5	Chemical shift-selective spin-echo imaging	17.6 Tesla (750 MHz)	80 μm isotropic	Horn et al. (2012)
Sunflower seed (*Helianthus annuus*)	4	Chemical shift-selective spin-echo imaging	9.4 Tesla (400 MHz)	47 × 47 μm^2 (500 μm)	Lakshminarayana et al. (1992)
Rapeseed seed	3	Water-suppressed spin-echo imaging	11.7 Tesla (500 MHz)	30 × 30 μm^2 (105 μm)	Neuberger et al. (2009)
Tobacco seed (*N. tabacum*)	0.7	Spin-echo imaging on dry seeds	17.6 Tesla (750 MHz)	25 μm isotropic	This study

to seed, the integrated data set obtained from a large population of seeds has provided a global picture in tobacco: In the endosperm, the highest level of lipid was associated with the region surrounding the embryonic radicle and in large cells, while in the embryo, most of the lipid present was deposited in the radicle/hypocotyl. The embryo in various species accumulates significant quantities of lipid (barley [*Hordeum vulgare*], Neuberger et al., 2008; rapeseed [*Brassica napus*], Neuberger et al., 2009; cotton [*Gossypium hirsutum*], Horn et al., 2012; soybean [*Glycine max*], Borisjuk et al., 2005; and oat [*Avena sativa*], Hayden et al., 2011) but commonly shows completely different gradients in oil distribution compared with tobacco. In dicotyledonous species, the embryo lipid concentrations are generally highest in the cotyledons, and in the monocotyledonous, the preferred site is its analog scutellum. In tobacco, the major site of accumulation in the embryo was the radicle, but, as in a number of other species, in particular jatropha (*Jatropha curcas*, Gu et al., 2012), oat (Hayden et al., 2011), and castor bean (*Ricinus communis*, Brown et al., 2012), most of the lipid in the seed was deposited in the endosperm.

The NMR platform provided a tool to show that the ratio between the volumes of the endosperm and the embryo differs between the cultivated species of tobacco *N. tabacum* and its ancestral species *N. sylvestris* (maternal progenitor) and *N. tomentosiformis* (paternal progenitor). Molecular diversity and contribution of parent genomes have been reported in a number of studies (Ren and Timko, 2001; Fricano et al., 2012), while seed architecture and lipid topology received much less attention. We created seed models of all three tobacco species, which differed by size and lipid content (Fig. 6). Seeds of both wild tobacco progenitors are smaller in size and comprise at least 2-fold higher endosperm/embryo ratios compared with *N. tabacum*. With respect to seed type, this observation is in agreement with general trends in angiosperm seed evolution, namely, that seeds with small embryo and abundant endosperm are rather primitive and evolution shows a general trend toward mature seeds with little or no endosperm in which the embryo occupies most of the seed (Finch-Savage and Leubner-Metzger, 2006). The imaging approach presented here offers a ready method of relating topological, biochemical, and molecular approaches, creating a comprehensive view of seed biodiversity and evolution.

NMR Analysis Indicates a Trade Off between Seed Size and Lipid Level in the Tobacco Seed

The NMR platform was able to simultaneously monitor seed size along with its lipid content in tobacco. This advantageous feature can be exploited for the analysis of mutant or transgenic individuals in which lipid content, seed production, and seed architecture are potentially altered. An example of such an analysis was provided by monitoring the consequences of heterologously expressing *BoPPT1* in the tobacco seed. In these seeds, it was possible to detect not just an altered level of lipid deposition, but also the localized accumulation of lipid in distinct regions of the endosperm and embryo.

In the Brassicaceae species oilseed rape and Arabidopsis, phospho*enol*pyruvate is believed to be an important precursor of fatty acid synthesis (Schwender and Ohlrogge, 2002; Andre and Benning, 2007; Lonien and Schwender, 2009). The supply of this metabolite from the cytosol to the plastid is catalyzed by PPT (Knappe et al., 2003), which, at least in soybean seed, is present at the same site as lipid accumulates (Borisjuk et al., 2005). In Arabidopsis, the down-regulation of PPT depresses lipid accumulation (Prabhakar et al., 2010). Our work demonstrated that its up-regulation raised lipid accumulation by approximately 13%. However, given PPT's proposed metabolite translocator function (and, hence, its importance for lipid synthesis; see Linka and Weber, 2010), the observed increase in seed lipid content was rather modest. Thus, it is likely, as suggested by Hayden et al. (2011), that other factors, such as the availability of specific intermediates and cofactors, must act to limit lipid storage in the seed. Metabolic control theory (as well as recent data provided by Lonien and Schwender [2009]) suggests that major perturbations of a single step have a lesser impact than do multiple, smaller ones. Therefore, the conclusion is that the up-regulation of PPT will need to be combined with additional interventions where the aim is to further improve the lipid storage capability of the tobacco seed.

The NMR imaging analysis revealed a strong negative correlation between seed size and lipid concentration (Fig. 7E). Assuming that seed metabolism is source limited and that a number of biosynthetic pathways compete with one another for a common substrate (s), any increase in lipid content would be expected to negatively impact seed size. The up-regulation of PPT, a key component of carbon delivery to the plastid, intensified this competition, resulting in a higher lipid concentration but a smaller seed. While seed number per capsule was unaffected by the presence of the *BoPPT1* transgene (data not shown), an alteration in the physiological and developmental regulation of lipid accumulation in the seeds (Baud and Lepiniec, 2010) cannot be excluded. Thus, a trade off between growth and storage during the course of seed development is likely to be one of the determinants of lipid yield.

MATERIALS AND METHODS

Plant Materials

Investigated tobacco (*Nicotiana* spp.) seeds of 36 accessions belonging to 10 *Nicotiana* wild species and 28 accessions of cultivated tobacco (*Nicotiana tabacum*) were obtained from the GenBank collection maintained at the Leibniz-Institut für Pflanzengenetik und Kulturpflanzenforschung. Details including the geographical origins are given in Supplemental Table S1. Nine wild species were represented by three accessions each. For *Nicotiana rustica*,

nine accessions belonging to three different varieties (var *asiatica*, var *brasilia*, var *rustica*) described by Danert (1963) were considered. For *N. tabacum*, we followed the nomenclature of Danert (1961), dividing the species into 10 varieties. All 10 varieties were considered. For var *alipes* and var *sagittata*, only two samples were available in the GenBank collection, whereas all others were represented by three accessions.

NMR Techniques

Hardware

For the low-field NMR experiments, a Bruker MQ60 was used. The NMR instrument has a magnetic field strength of 1.5 Tesla. The probe head allows for analyzing samples with a diameter of up to 5 mm and a length of 1 cm. All high-field experiments were conducted on a vertical 17.6-Tesla Bruker Avance II wide-bore system operating at 750 MHz. The Micro 2.5 gradient set (Bruker) had an i.d. of 40 mm and a maximum gradient strength of 1 Tesla m^{-1}.

High-Throughput Quantification of Oil Content Using Low-Field TD-NMR

The determination of lipid content using low-field TD-NMR (using MQ60) is based on detecting the spin echo at 7-ms echo time (TE). Mature intact seeds were loaded into the tubes at 20°C, and the spin-echo signal was averaged over 16 measurements. The signal height of the spin echo is proportional to lipid content in seeds (Borisjuk et al., 2011; Horn et al., 2011b), given that seeds are dry. The proportionality constant was estimated from a range of samples with known lipid content. About 20 mg of seed was used for individual measurements (with up to eight replicates each). Additionally, following the NMR analysis, seed and some tobacco leaf samples were powdered to obtain conventional estimates of their total lipid content (using gas chromatography). Both noninvasive and conventional assays were superposed (Supplemental Fig. S2). A high correlation between the independent measurement methods was achieved. Therefore, low-field NMR enables accurate, rapid quantification of lipid content. Notably, the NMR analysis takes approximately 1 min per sample and thus allows high-throughput applications.

Two-Dimensional Multislice Imaging of the Capsule

A spin-echo sequence with a frequency-selective VAPOR suppression preparation module was used to acquire the MRI data. An in-house-built 20-mm-i.d. birdcage resonator was used for data acquisition. In detail, the VAPOR suppression parameters were adjusted using global spectroscopic measurements. The transmitting frequency was set on resonant of water. For water suppression, a bandwidth of 3000 Hz with an offset of 500 Hz (away from the lipid signal) was used, and the pulse powers were manually adjusted to achieve optimal water signal suppression. The same procedure was carried out for lipid suppression (bandwidth, 2000 Hz; offset, −2,500 Hz). The repetition time (TR) was 3000 ms in both experiments, allowing almost complete T1 relaxation. The TE was kept as short as possible (6.2 ms) to minimize effects of T2 relaxation. During one repetition, 33 slices with a slice thickness of 750 μm were acquired. With a field of view (FOV) of 12 × 12 mm^2 and a matrix size of 192 × 192, an isotropic in plane resolution of 62 μm could be achieved. Averaging the experiment six times resulted in a total experimental time of 57 min for each scan. This approach was applied to create data sets for Figure 2, B and C, and Figure 3, B to D.

Three-Dimensional Imaging of the Capsule

A chemical shift-selective spin-echo sequence (TE = 6.5 ms and TR = 2000 ms, two averages) was used to visualize the whole fruit (Neuberger et al., 2008). The signals from water and lipid were acquired in an interleaved manner during the experiment time of about 18 h. Chemical shift-selective hermite pulses with a bandwidth of 2000 Hz were used for global excitation and refocusing of the protons. The pulses were given on-resonance for water to acquire water images and with an offset of −2,800 Hz to generate lipid images. An isotropic resolution of 109 μm (FOV = 28 × 14 × 14 mm^3, matrix = 256 × 128 × 128) was achieved for both the water and the lipid data sets. By interleaving the water and lipid acquisitions, the scan time could be reduced by a factor of two, compared with a sequential acquisition of water and lipid with the same TR. This method was used to acquire the data sets for Figure 4B. In-house Java-based software was used for data reconstruction, while the visualization of the capsule was performed with AMIRA software (VSG). The estimation of the seed number was derived from image segmentation using AMIRA.

Three-Dimensional Imaging of Single Tobacco Seed

A standard three-dimensional spin-echo sequence was used to acquire images from the lipid distribution of single dried tobacco seeds. A water suppression module was not necessary as the residual bound water did not contribute any detectable signal. The experiments were carried out using a 2-mm-i.d. solenoid coil. With an FOV of 4 × 4 × 1 mm^3 and a matrix size of 160 × 160 × 40, an isotropic resolution of 25 μm could be achieved. The shortest possible TE was 6.4 ms. With two averages and a TR of 3000 ms, the data set was acquired in <11 h. This technique was used to acquire the data sets for Figure 5. In-house software was used for data reconstruction, while the visualization and manual segmentation for modeling was performed with AMIRA. For Figure 6, D to L, a similar sequence was used with the following parameters: TE 6.5 ms, matrix 350 × 140 × 140, FOV 12.5 × 5 × 5 mm, isotropic resolution 36 μm, TR 3500 ms, two averages, and 36-h total measurement time.

Three-Dimensional Imaging of Multiple Seeds and Computation of the Virtual Model Seeds

For sample preparation and data acquisition, two different types of seeds (transgenic PPT7 line and the wild type) of mature seeds were examined in this experiment. While one of them (PPT7) was placed inside a 3-mm NMR tube (2.5-mm i.d.), the other species (the wild type) was poured carefully around the 3-mm NMR tube after it was inserted into a 5-mm NMR tube (4-mm i.d.). Both of the NMR tubes were filled with vegetable oil for B1 correction and calibration. The complete sample was placed into an in-house-built 5-mm scroll coil (Hayes et al., 1985; Grant et al., 2001). As no water signal was present, a standard three-dimensional spin-echo sequence (TR = 1750 ms, TE = 5.7 ms, FOV = 9 × 4.5 × 4.5 mm^3, matrix size = 320 × 160 × 160) without a suppression module could be used to acquire data sets with a 28-μm isotropic resolution. The total experimental time was 25 h.

Data Reconstruction and Analysis

The acquired data set was zero filled by a factor of three in each direction before it was reconstructed by a three-dimensional inverse fast Fourier transformation using our software. To exclude strong B1 inhomogeneity at the side of the three-dimensional data set along the axis of the scroll coil and artifacts caused by insufficient filtering in the frequency (readout) direction, the data set was cropped to a size of 768 × 480 × 480 voxels.

To correct the data for the residual B1 inhomogeneity within the data set, a calibration had to be applied. This correction could be performed using the external vegetable oil, which also served as a known standard (density 0.9 μg/nL) to calibrate the signal values (after T1 and T2 correction for seeds and the oil). Therefore, the data set was split into several regions with obvious different B1 values. As the pure oil produced higher signal intensity than the seeds, a threshold accepting method (AMIRA) could be applied in each region to separate the seeds from the vegetable oil. Using in-house software written in Java, the pure oil signal was used to calibrate for signal changes due to B1 differences along the axis of the coil. As the B1 homogeneity perpendicular to the axis of the coil was within an acceptable range <5%, no B1 correction needed to be applied in these directions.

To be able to create an "average seed," all seeds needed to be detected as single entities. As some of the seeds were touching each other, a method to separate them needed to be developed. A shrinking algorithm was applied to a mask containing only the voxels of the seeds. As soon as the seeds were separated, each seed was given a distinct number and the individual seed regions were grown again to fill the original seed mask. Finally, to keep the seed regions separate from each other, the regions were shrunk by two voxels, which is less than one voxel of the non-zero-filled data set. Furthermore, this approach avoids leaking of pure oil signal from the surrounding oil into the seeds. After the segmentation and calibration, the total oil content and the volume of each seed could be determined.

To create a "virtual model seed," the spatial distributions of the resulting seed regions were examined using the eigenvalues and eigenvectors of their covariance matrix. Due to their elliptical shape, these eigenvectors can be used to determine the orientation of the individual seeds. To find the top and the

bottom of the seed within the ellipsoidal shape, a small region above and below the center was analyzed and depending on the oil content the seed was flipped vertically. Around 100 seeds per species were aligned and averaged to create the seed models shown in Figure 7, C and D.

Using Mathematica (Wolfram Research), the ellipses in Figure 7, E and F, were calculated from the covariance matrix of the size and lipid concentration data. The size of the ellipses is determined by SD of the principal components (dark gray 1 σ; light gray 2 σ), and the obliqueness of the ellipse (angle between the axes of the ellipse and the axes of the coordinate system) indicates the correlation between the size and the lipid concentration of the seed specimen.

Generation of Transgenic Tobacco Plants and Fatty Acid Analysis in Seeds

The full-length complementary DNA of *Brassica oleracea* nongreen plastid phospho*enol*pyruvate/phosphate translocator (BoPPT; EMBL accession number U13632) has been provided by U.-L. Flügge (Fischer et al., 1997). The BoPPT1 complementary DNA fragment was cloned between the LegB4 promoter from *Vicia faba* (Bäumlein et al., 1991) and 3′-region of octopine synthase (ocs) terminator, resulting in the expression cassette LegB4P/BoPPT1/ocs. To generate a binary vector, the LegB4P/BoPPT1/ocs was cloned into pGPTV-bar (Becker et al., 1992) plasmid replacing the GUS gene cassette. All plasmid manipulations were carried out according to the methods described by Sambrook et al. (1989). The resulting plasmid was transformed into *Agrobacterium tumefaciens* strain EHA105 and transferred into tobacco 'SNN' according to the method of Horsch et al. (1985).

The presence of PPT expression cassette in transformed tobacco lines was confirmed by PCR analysis of isolated genomic DNA using primers binding at 3′-region of LegB4 promoter and 5′-region of BoPPT1 gene sequences (5′-CACACACGTTCTGTCACACG-3′ for LeB4 and 5′-ACTGCCGTAGCTG-CAGTTTT-3′ for PPT). More than 90% of tobacco lines selected on kanamycin showed the presence of gene-specific PCR fragments. Tobacco PPT plants were further analyzed for the presence of introduced cassette by Southern DNA analysis, and the expression of BoPPT1-specific mRNA was confirmed by northern analysis (Supplemental Fig. S1A). Analysis of fatty acid composition in seeds of tobacco plants was performed by gas chromatography as previously described (Borisjuk et al., 2005).

Supplemental Data

The following materials are available in the online version of this article.

Supplemental Figure S1. Analysis of transgenic tobacco plants heterologously expressing the *B. oleracea* gene *BoPPT1*.

Supplemental Figure S2. TD-NMR-based measurement of the lipid content of tobacco leaf and seed tissue is consistent with NMR and gas chromatography-based data.

Supplemental Table S1. *Nicotiana* spp. accessions sampled from the IPK GenBank collection.

Supplemental Movie S1. Visualization of water (right) and lipid (left) distribution in the tobacco capsule.

Supplemental Movie S2. Three-dimensional model of the tobacco capsule.

Supplemental Movie S3. Three-dimensional model of the tobacco seed, showing the embryo (green) surrounded by endosperm.

Supplemental Movie S4. Topology of lipid accumulation in the embryo of a tobacco seed.

Supplemental Movie S5. Topology of lipid accumulation in the endosperm of a tobacco seed.

ACKNOWLEDGMENTS

We thank Prof. T. Altmann for discussion and support, Dr. R. Radchuk for help with the molecular analysis, and S. Wagner, S. Ortleb, and S. Herrmann for technical assistance.

Received October 30, 2012; accepted December 4, 2012; published December 11, 2012.

LITERATURE CITED

Agrawal P, Verma D, Daniell H (2011) Expression of *Trichoderma reesei* β-mannanase in tobacco chloroplasts and its utilization in lignocellulosic woody biomass hydrolysis. PLoS ONE **6:** e29302

Andre C, Benning C (2007) Arabidopsis seedlings deficient in a plastidic pyruvate kinase are unable to utilize seed storage compounds for germination and establishment. Plant Physiol **145:** 1670–1680

Andrianov V, Borisjuk N, Pogrebnyak N, Brinker A, Dixon J, Spitsin S, Flynn J, Matyszczuk P, Andryszak K, Laurelli M, et al (2010) Tobacco as a production platform for biofuel: Overexpression of *Arabidopsis* DGAT and LEC2 genes increases accumulation and shifts the composition of lipids in green biomass. Plant Biotechnol J **8:** 277–287

Baud S, Lepiniec L (2009) Regulation of *de novo* fatty acid synthesis in maturing oilseeds of *Arabidopsis*. Plant Physiol Biochem **47:** 448–455

Baud S, Lepiniec L (2010) Physiological and developmental regulation of seed oil production. Prog Lipid Res **49:** 235–249

Bäumlein H, Boerjan W, Nagy I, Panitz R, Inzé D, Wobus U (1991) Upstream sequences regulating legumin gene expression in heterologous transgenic plants. Mol Gen Genet **225:** 121–128

Becker D, Kemper E, Schell J, Masterson R (1992) New plant binary vectors with selectable markers located proximal to the left T-DNA border. Plant Mol Biol **20:** 1195–1197

Bindler G, Plieske J, Bakaher N, Gunduz I, Ivanov N, Van der Hoeven R, Ganal M, Donini P (2011) A high density genetic map of tobacco (*Nicotiana tabacum* L.) obtained from large scale microsatellite marker development. Theor Appl Genet **123:** 219–230

Borisjuk L, Nguyen TH, Neuberger T, Rutten T, Tschiersch H, Claus B, Feussner I, Webb AG, Jakob P, Weber H, Wobus U, Rolletschek H (2005) Gradients of lipid storage, photosynthesis and plastid differentiation in developing soybean seeds. New Phytol **167:** 761–776

Borisjuk L, Rolletschek H, Fuchs J, Melkus G, Neuberger T (2011) Low and high field magnetic resonance for *in vivo* analysis of seeds. Materials **4:** 1426–1439

Borisjuk L, Rolletschek H, Neuberger T (2012) Surveying the plant's world by magnetic resonance imaging. Plant J **70:** 129–146

Borisjuk NV, Borisjuk LG, Logendra S, Petersen F, Gleba Y, Raskin I (1999) Production of recombinant proteins in plant root exudates. Nat Biotechnol **17:** 466–469

Brescia MA, Pugliese T, Hardy E, Sacco A (2007) Compositional and structural investigations of ripening of table olives, Bella della Daunia, by means of traditional and magnetic resonance imaging analyses. Food Chem **105:** 400–404

Brown AP, Kroon JT, Swarbreck D, Febrer M, Larson TR, Graham IA, Caccamo M, Slabas AR (2012) Tissue-specific whole transcriptome sequencing in castor, directed at understanding triacylglycerol lipid biosynthetic pathways. PLoS ONE **7:** e30100

Danert S (1961) Zur Systematik von *Nicotiana tabacum* L. Kulturpflanze **9:** 287–363

Danert S (1963) Zur Systematik von *Nicotiana rustica* L. Kulturpflanze **11:** 535–562

Davoodi-Semiromi A, Samson N, Daniell H (2009) The green vaccine: a global strategy to combat infectious and autoimmune diseases. Hum Vaccin **5:** 488–493

Finch-Savage WE, Leubner-Metzger G (2006) Seed dormancy and the control of germination. New Phytol **171:** 501–523

Fischer K, Kammerer B, Gutensohn M, Arbinger B, Weber A, Häusler RE, Flügge UI (1997) A new class of plastidic phosphate translocators: a putative link between primary and secondary metabolism by the phosphoenolpyruvate/phosphate antiporter. Plant Cell **9:** 453–462

Frega N, Bocci F, Conte L, Testa F (1991) Chemical composition of tobacco seeds (*Nicotiana tabacum* L.). J Am Oil Chem Soc **68:** 29–33

Fricano A, Bakaher N, Del Corvo M, Piffanelli P, Donini P, Stella A, Ivanov NV, Pozzi C (2012) Molecular diversity, population structure, and linkage disequilibrium in a worldwide collection of tobacco (*Nicotiana tabacum* L.) germplasm. BMC Genet **13:** 18

Gadani F, Hayes A, Opperman C, Lommel S, Sosinski B, Burke M, Hi L, Brierly R, Salstead A, Heer J, et al (2003) Large scale genome sequencing and analysis of *Nicotiana tabacum*: the tobacco genome initiative. *In* Proceedings of the 5émes Journées Scientifiques du Tabac de Bergerac, Bergerac, France, pp 117–130

Grant S, Murphy L, Magin R, Friedman G (2001) Analysis of multilayer radio frequency microcoils for nuclear magnetic resonance spectroscopy. IEEE Trans Magn **37:** 2989–2998

Gu K, Yi C, Tian D, Sangha JS, Hong Y, Yin Z (2012) Expression of fatty acid and lipid biosynthetic genes in developing endosperm of *Jatropha curcas*. Biotechnol Biofuels **5:** 47–62

Halloin JM, Cooper TG, Potchen EJ, Thompson TE (1993) Proton magnetic resonance imaging of lipid in pecan embryos. J Am Oil Chem Soc **70:** 1259–1262

Hayden DM, Rolletschek H, Borisjuk L, Corwin J, Kliebenstein DJ, Grimberg A, Stymne S, Dehesh K (2011) Cofactome analyses reveal enhanced flux of carbon into oil for potential biofuel production. Plant J **67:** 1018–1028

Hayes CE, Edelstein WA, Schenck JF, Mueller OM, Eash M (1985) An efficient, highly homogenous radiofrequency coil for whole-body NMR imaging at 1.5 T. J Magn Reson **63:** 622–628

Horn PJ, Korte AR, Neogi PB, Love E, Fuchs J, Strupat K, Borisjuk L, Shulaev V, Lee YJ, Chapman KD (2012) Spatial mapping of lipids at cellular resolution in embryos of cotton. Plant Cell **24:** 622–636

Horn PJ, Ledbetter NR, James CN, Hoffman WD, Case CR, Verbeck GF, Chapman KD (2011a) Visualization of lipid droplet composition by direct organelle mass spectrometry. J Biol Chem **286:** 3298–3306

Horn PJ, Neogi P, Tombokan X, Ghosh S, Campbell BT, Chapman KD (2011b) Simultaneous quantification of oil and protein in cottonseed by low-field time-domain nuclear magnetic resonance. J Am Oil Chem Soc **88:** 1521–1529

Horsch R, Fry J, Hoffmann N, Eichholtz D, Rogers SG, Fraley R (1985) A simple and general method for transferring genes into plants. Science **227:** 1229–1231

Jagannathan NR, Govindaraju V, Raghunathan P (1995) *In vivo* magnetic resonance study of the histochemistry of coconut (*Cocos nucifera*). Magn Reson Imaging **13:** 885–892

Knappe S, Flügge UI, Fischer K (2003) Analysis of the plastidic phosphate translocator gene family in Arabidopsis and identification of new phosphate translocator-homologous transporters, classified by their putative substrate-binding site. Plant Physiol **131:** 1178–1190

Lakshiminarayana MR, Joshi S, Gowda GAN, Khetrapal CL (1992) Spatial distribution of oil in groundnut and sunflower seeds by nuclear magnetic resonance imaging. J Biosci **17:** 87–93

Linka N, Weber APM (2010) Intracellular metabolite transporters in plants. Mol Plant **3:** 21–53

Lonien J, Schwender J (2009) Analysis of metabolic flux phenotypes for two Arabidopsis mutants with severe impairment in seed storage lipid synthesis. Plant Physiol **151:** 1617–1634

Manz B, Müller K, Kucera B, Volke F, Leubner-Metzger G (2005) Water uptake and distribution in germinating tobacco seeds investigated *in vivo* by nuclear magnetic resonance imaging. Plant Physiol **138:** 1538–1551

Melkus G, Rolletschek H, Radchuk R, Fuchs J, Rutten T, Wobus U, Altmann T, Jakob P, Borisjuk L (2009) The metabolic role of the legume endosperm: a noninvasive imaging study. Plant Physiol **151:** 1139–1154

Morandini F, Avesani L, Bortes L, Van Droogenbroeck B, De Wilde K, Arcalis E, Bazzoni F, Santi L, Brozzetti A, Falorni A, et al (2011) Non-food/feed seeds as biofactories for the high-yield production of recombinant pharmaceuticals. Plant Biotechnol J **9:** 911–921

Neuberger T, Rolletschek H, Webb A, Borisjuk L (2009) Non-invasive mapping of lipids in plant tissue using magnetic resonance imaging. Methods Mol Biol **579:** 485–496

Neuberger T, Sreenivasulu N, Rokitta M, Rolletschek H, Göbel C, Rutten T, Radchuk V, Feussner I, Wobus U, Jakob P, et al (2008) Quantitative imaging of oil storage in developing crop seeds. Plant Biotechnol J **6:** 31–45

Patel JA, Patel BK, Chakraborty MK (1998) Production potential and quality aspects of tobacco seed oil. Tobacco Research **24:** 44–49

Prabhakar V, Löttgert T, Geimer S, Dörmann P, Krüger S, Vijayakumar V, Schreiber L, Göbel C, Feussner K, Feussner I, et al (2010) Phosphoenolpyruvate provision to plastids is essential for gametophyte and sporophyte development in *Arabidopsis thaliana*. Plant Cell **22:** 2594–2617

Ren N, Timko MP (2001) AFLP analysis of genetic polymorphism and evolutionary relationships among cultivated and wild *Nicotiana* species. Genome **44:** 559–571

Sambrook J, Fritsch E, Maniatis T (1989) Isolation of bacteriophage and plasmid DNA. *In* Molecular Cloning: A Laboratory Manual. Cold Spring Harbor Laboratory Press, Cold Spring Harbor, NY, pp 86–96

Schiebold S, Tschiersch H, Borisjuk L, Heinzel N, Radchuk R, Rolletschek H (2011) A novel procedure for the quantitative analysis of metabolites, storage products and transcripts of laser microdissected seed tissues of *Brassica napus*. Plant Methods **7:** 19

Schillberg S, Fischer R, Emans N (2003) Molecular farming of recombinant antibodies in plants. Cell Mol Life Sci **60:** 433–445

Schwender J, Ohlrogge JB (2002) Probing in vivo metabolism by stable isotope labeling of storage lipids and proteins in developing *Brassica napus* embryos. Plant Physiol **130:** 347–361

Seongjin C (2008) Proton NMR and MRI studies of sub-millimeter sized biological object. PhD thesis. The Ohio State University, Columbus, OH

Terskikh VV, Feurtado JA, Ren C, Abrams SR, Kermode AR (2005) Water uptake and oil distribution during imbibition of seeds of western white pine (*Pinus monticola* Dougl. ex D. Don) monitored *in vivo* using magnetic resonance imaging. Planta **221:** 17–27

Tkác I, Starcuk Z, Choi IY, Gruetter R (1999) *In vivo* ^{1}H NMR spectroscopy of rat brain at 1 ms echo time. Magn Reson Med **41:** 649–656

Tomlinson KL, McHugh S, Labbe H, Grainger JL, James LE, Pomeroy KM, Mullin JW, Miller SS, Dennis DT, Miki BL (2004) Evidence that the hexose-to-sucrose ratio does not control the switch to storage product accumulation in oilseeds: analysis of tobacco seed development and effects of overexpressing apoplastic invertase. J Exp Bot **55:** 2291–2303

Usta N (2005) Use of tobacco seed oil methyl ester in a turbocharged indirect injection diesel engine. Biomass Bioenergy **28:** 77–86

Verma D, Kanagaraj A, Jin S, Singh ND, Kolattukudy PE, Daniell H (2010) Chloroplast-derived enzyme cocktails hydrolyse lignocellulosic biomass and release fermentable sugars. Plant Biotechnol J **8:** 332–350

Wallis JG, Browse J (2010) Lipid biochemists salute the genome. Plant J **61:** 1092–1106

Zagorevski DV, Loughmiller-Newman JA (2012) The detection of nicotine in a Late Mayan period flask by gas chromatography and liquid chromatography mass spectrometry methods. Rapid Commun Mass Spectrom **26:** 403–411

Zambryski P, Joos H, Genetello C, Leemans J, Montagu MV, Schell J (1983) Ti plasmid vector for the introduction of DNA into plant cells without alteration of their normal regeneration capacity. EMBO J **2:** 2143–2150